Diffraction at CMS

Wagner de Paula Carvalho[1] , for The CMS Collaboration

[1]Universidade do Estado do Rio de Janeiro, Rua Sao Francisco Xavier 524, 20559-900 Rio de Janeiro, Brazil

A summary of studies on diffraction with CMS detector and of planned measurements with early CMS data is presented.

1 Introduction

A long term program in Forward Physics is envisaged to be carried out with CMS [1]. Inclusive single diffraction (SD) and double pomeron exchange (DPE) at low luminosities, diffraction in the presence of a hard scale (jets, heavy quarks, vector bosons) at moderate luminosities and central exclusive production at the highest luminosities are some of the topics to be pursued.

LHC is expected to deliver a few hundred pb^{-1} over its first running period, scheduled to start by the end of this year. With such amount of data collected under low instantaneous luminosity conditions, a variety of studies will become accessible: observation of hard diffractively produced W bosons and di-jets; assessment of the rapidity gap survival probability at LHC energies; probing of the diffractive parton distribution functions (PDF); observation of exclusively photoproduced Υ and study of its production dynamics.

2 Forward Detectors at CMS

Although there are plans to add proton tagging detectors to CMS, in the near future all diffractive analyses will have to rely on the rapidity gap signature and the coverage provided by the most forward CMS subsystems: the Hadronic Forward (HF), CASTOR and Zero Degree (ZDC) calorimeters.

Located at 11.2m from the interaction point (IP), at both sides of CMS, the HF is a steel/quartz fibre calorimeter covering the pseudorapidity range $3.0 < |\eta| < 5.0$. It is $\eta - \phi$ segmented, amounting to 900 towers of typical size 0.175×0.175.

CASTOR (Centauro And STrange Object Research) is a tungsten/quartz plates calorimeter, placed 14.3 m away from the IP. It is longitudinally and azimuthally segmented, but has no segmentation in η. The azimuthal segmentation defines 16 sectors. For the LHC start, there will have only one CASTOR, covering the pseudorapidity region $-6.6 < \eta < -5.2$.

ZDC is also a tungsten/quartz calorimeter, located 140m away from the IP at both sides of CMS. It will measure very forward photons and neutrons at $|\eta| > 8.1$.

Further details about these subsystems or CMS apparatus can be found elsewhere [2].

3 Studies in Preparation for Data

In this section we present prospective studies based on Monte Carlo simulations for diffractive processes at CMS. These studies were performed in preparation for the LHC start up. A scenario with centre-of-mass energy of 14 TeV and no pile-up was assumed.

3.1 Single Diffractive Production of W Bosons and Di-Jets

The single diffractive (SD) production of W bosons and of di-jets are both hard diffractive processes, characterised by the presence of a hard scale and a large rapidity gap (LRG) in the final state. These processes are sensitive to the diffractive structure function of the proton; the W production is mainly sensitive to its quark content and the di-jet is sensitive to its gluon content.

Both analyses, described in details in references [3, 4], used samples produced under similar conditions and the same methodology.

3.1.1 Monte Carlo Simulation

In order to simulate the SD process, the POMWIG generator [5], v2.0 beta, was used. For the diffractive PDF and Pomeron flux, the NLO H1 2006 fit B [6] was used, while for the proton PDF, the CTEQ6 [7] parametrisation was adopted. A rapidity gap survival probability ($\langle|S^2|\rangle$) of 0.05 was assumed [8]. The non-diffractive background was simulated by PYTHIA [9] for W production and by MADGRAPH [10] for the di-jet production. All samples were subject to full detector simulation, trigger emulation and reconstruction. The CASTOR information, however, is treated at generator level as this subsystem was not included in the full simulation chain.

3.1.2 Event Selection

W or di-jet candidates are selected by applying standard trigger and offline requirements. For $W \to \mu\nu$ selection, the same criteria of reference [11] was used. Basically, to be accepted an event was required to have one muon candidate in $|\eta| < 2.0$ and with $p_T > 25\,\text{GeV}$. It should also have a transverse mass $M_T > 50\,\text{GeV}$. Additional muon isolation cuts and cuts to reject contributions from top quark were applied. Events with more than one muon candidate with $p_T > 20\,\text{GeV}$ were rejected. For di-jets, at the trigger level events were selected by requiring at least 2 jets with average uncorrected transverse energy greater than 30 GeV. Jets were reconstructed with the SiSCone5 [12] algorithm and jet-energy scale corrections were applied. Finally, at least two jets with $E_T > 55\,\text{GeV}$ were required.

3.1.3 Gap Side Definition and Central Track Multiplicity

On average, SD events have less particles and energy deposited in the side that contains the scattered proton, when compared to non-diffractive events. This becomes clear from the generated energy-weighted η distribution for stable particles (excluding neutrinos) in diffractive and non-diffractive $W \to \mu\nu$ events, shown in Figure 1 (also shown in this figure is the η range covered by HF and CASTOR). In order to select diffractive candidates, a *gap side* was defined as the side with the lowest energy sum in HF. When applied to simulated SD samples, this definition wrongly selected the gap side (side of the scattered proton) $\sim 30\%$ of times for $W \to \mu\nu$

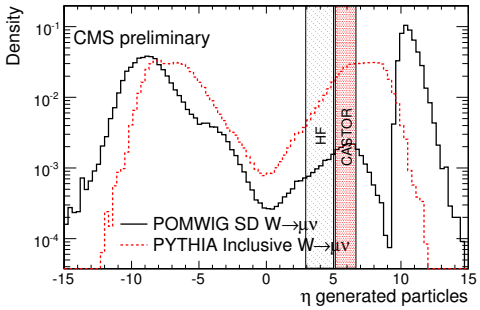

Figure 1: Generated energy-weighted η distribution for stable particles (excluding neutrinos) in diffractive and non-diffractive $W \to \mu\nu$ events. The peak at $\eta >\sim 10$ for the diffractive sample corresponds to the scattered proton.

events and $\sim 10\%$ of times for di-jet events. One additional cut was applied to the di-jet candidates, exploiting the anti correlation between gap side and jets side: if the gap is found to be at positive rapidity, the two leading jets are required to be in the range $-4 < \eta_{jet} < 1$, otherwise, if the gap is at negative rapidity, the two leading jets are then required to be in the range $-1 < \eta_{jet} < 4$. Finally, a cut on the maximum η separation between the two leading jets was applied: $|\Delta\eta_{jets}| < 3$.

The track multiplicity in the central region can also be used for discriminating diffractive and non-diffractive events. Figure 2 shows the multiplicity distribution for tracks with $p_T > 900\,\text{MeV}$. Diffractive events have a distribution that peaks at zero, contrary to non-diffractive events, and this feature was exploited for introducing a multiplicity cut for tracks with $|\eta_{tracks}| < 2$. Three values were used for these studies: $N_{tracks} \leq 1$, $N_{tracks} \leq 5$ and no cut at all.

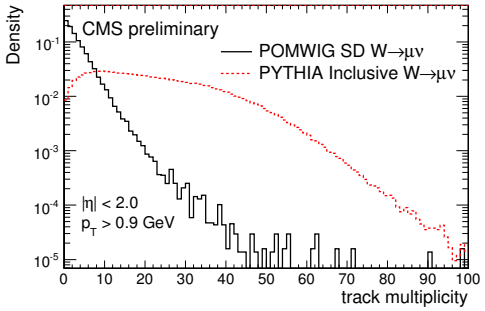

Figure 2: Central tracker multiplicity distributions for diffractively and non-diffractively produced $W \to \mu\nu$ events, excluding the track from the μ candidate.

3.1.4 HF and CASTOR Multiplicity Distributions

For the events passing the selection criteria, two-dimensional (2D) distributions of the activity in the forward calorimeters (HF and CASTOR) were obtained and used to assess the possibility

of observing SD in early data, in a similar way to analyses carried out at the Tevatron and at HERA. For HF, activity was quantified by the number of towers with deposited energy above threshold. For CASTOR, the number of ϕ sectors hit by hadrons with energy above 10 GeV was used to this purpose. As there was no detector simulation/reconstruction implemented for this subsystem, the generated particle information was used in turn.

Two possible experimental scenarios were considered: *1)* no forward detectors beyond HF and *2)* additional η coverage provided by CASTOR.

In the first scenario, HF towers are grouped in two slices as a function of their η coordinate: "low-η slice" for $2.9 < |\eta| < 4.0$ and "forward slice" for $4.0 < |\eta| < 5.2$. Figure 3 shows the 2D tower multiplicity for $W \rightarrow \mu\nu$ events with $N_{tracks} \leq 5$. Top plots present the gap side multiplicity distributions for SD events with the generated gap in the positive (left) and negative (right) sides. They show a clear peak at the zero multiplicity bin. Conversely, the bottom left distribution for non-diffractive events shows no enhancement at the zero bin. The bottom right plot shows the sum of the two distributions, which are normalised to the same integrated luminosity of 100pb^{-1}. This is the kind of distribution expected from data. An excess due to diffractive signal is clearly visible at the zero multiplicity bin. This excess becomes even more significant as the central tracks multiplicity cut becomes stricter.

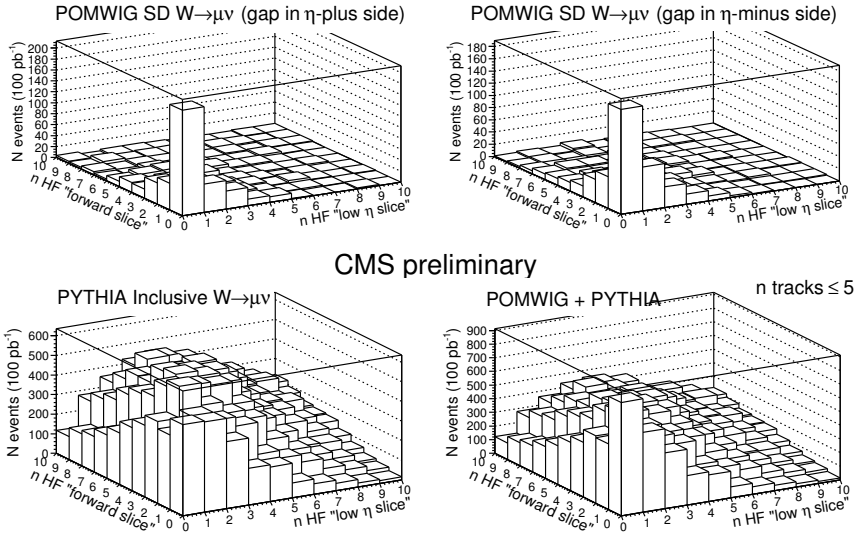

Figure 3: Tower multiplicity distributions in HF.

Similar distributions can be obtained when CASTOR is taken into consideration. Figure 4 shows the HF tower vs. CASTOR ϕ sector multiplicity distributions for $W \rightarrow \mu\nu$ events with $N_{tracks} \leq 5$. Because CASTOR will be available only in the negative side for the first running period, only events with gap in that side (as defined in Section 3.1.3 were considered). The top left plot shows those events for which the gap has been wrongly determined. The other plots are qualitatively analogous to those in Figure 3. With the extra coverage provided by CASTOR, the signal to background ratio (S/B) got greatly improved. For $N_{tracks} \leq 5$, the ratio is $\mathcal{O}(1)$ for HF-only and $\mathcal{O}(10)$ for HF-CASTOR.

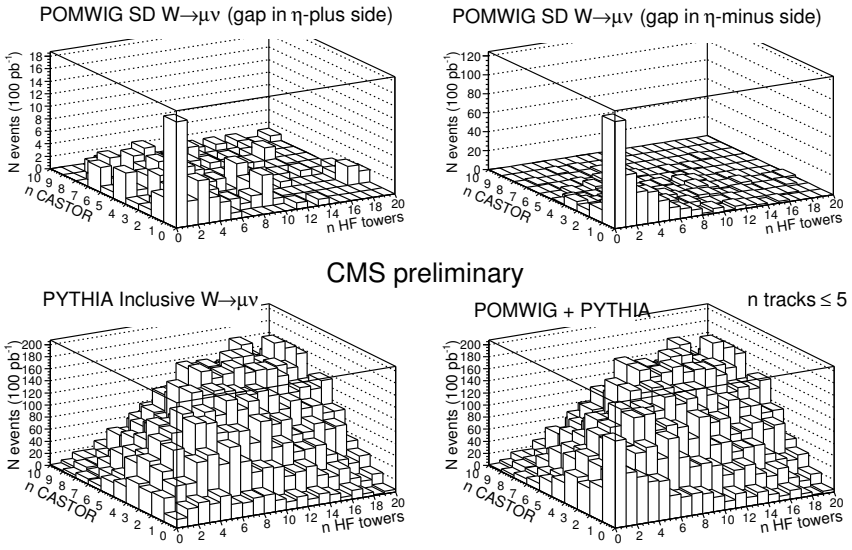

Figure 4: Multiplicity distributions for HF and CASTOR.

The same exercise was carried out for the SD di-jets. In the very same way, the addition of CASTOR results in a improvement by more than one order of magnitude of S/B.

3.1.5 Establishing Diffractive Signal in Data

The presence of a diffractive signal in data can be demonstrated without relying on MC. This can be achieved by varying the diffractive selection criteria and showing that the diffractive peak at zero multiplicity varies in a predictable way. Table 1 illustrates for SD di-jet production how S/B improves by tightening the central tracker multiplicity cut, even in the less favourable HF-only scenario. It must be pointed out that such behaviour is the opposite of what would be expected, were the excess due to a statistical fluctuation.

N_{tracks}^{max}	∞	5	1
S/B	0.6	0.9	1.3

Table 1: Evolution of S/B as a function of N_{tracks}^{max}, for SD di-jet production.

3.1.6 Feasibility Studies and Sensitivity to $\langle|S^2|\rangle$

One goal of these studies was determining the feasibility of observing SD production of di-jets and W, through its semileptonic decay $W \to \mu\nu$, with a limited sample of early CMS data. Under the simulated conditions, signals of $\mathcal{O}(400)$ events are expected in the SD di-jet channel with the first 10pb^{-1} and of $\mathcal{O}(100)$ events in the SD $W \to \mu\nu$ channel with the first 100pb^{-1}, if CASTOR is available.

Another possible result that can be achieved is exclude extreme values of the rapidity gap survival probability at LHC energies. Values as low as 0.004 and as high as 0.23 have been proposed [13]. Simulations show that these values would lead to marginally observable signals in the first case, only detectable by profiting of CASTOR extended η coverage, and to very prominent signals in the second case, easily detectable by HF alone. Measured event yields could eventually exclude these extreme values.

3.2 Exclusive Υ Photoproduction

The exclusive production of $\Upsilon \rightarrow \mu^+\mu^-$ through γp interaction, represented in Figure 5, is another diffractive process accessible with early CMS data. As for SD di-jets and W analyses, a scenario with centre-of-mass energy of 14 TeV and no pile-up was assumed in this study [14].

3.2.1 Monte Carlo Simulation and Event Selection

The signal samples were generated with STARLIGHT [15] adopting the following predicted values of cross-section times branching fraction for the first three Υ resonances (1S, 2S, 3S): 39.0 pb, 13.0 pb, and 10.0 pb. LPAIR [16] was used to simulate the inelastic two-photon events, while PYTHIA was used for all other backgrounds (Drell-Yan, quarkonium decays, heavy-flavor jets). All samples were subject to full detector simulation, trigger emulation and reconstruction.

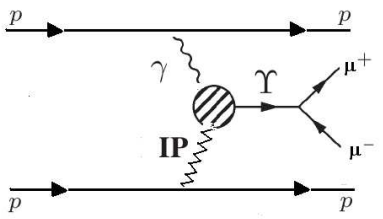

Figure 5: Feynman diagram for $\gamma p \rightarrow \Upsilon p \rightarrow \mu^+\mu^- p$.

At the trigger level, dimuon candidates were selected by requiring two muons with $p_T > 3$ GeV (high trigger thresholds essentially kill the corresponding dielectron channel). Major backgrounds were suppressed by cutting on the muon pair kinematics and on the additional detector activity. Dimuons were required to be well balanced in transverse momentum, satisfying the condition $|\Delta p_T(\mu^+\mu^-)| < 2.0$ GeV, and nearly back-to-back in the azimuthal angle, $|\Delta\phi(\mu^+\mu^-)| > 2.9$. A calorimeter exclusivity condition was applied by requiring less than 5 extra towers above noise threshold to be present in the event. Finally, no extra charged track, beyond the 2 muon candidates, was allowed in the event.

3.2.2 Dimuon Spectrum and Υ Yield

After all the selection and exclusivity conditions are applied, the dominant remaining background comes from inelastic photon-exchange events, in which the proton remnants lay outside HF coverage. However, a significant fraction of these events could be detected by CASTOR and ZDC detectors. Based on the generator level information and considering a configuration with CASTOR at only one side, it was estimated that approximately 2/3 of the remaining inelastic background could be rejected by vetoing on CASTOR and ZDC.

Figure 6 shows clearly visible signals for the first three Υ resonances with a simulated integrated luminosity of 100pb^{-1}. With such event yield, studies of the Υ production dynamics might even be possible with early CMS data.

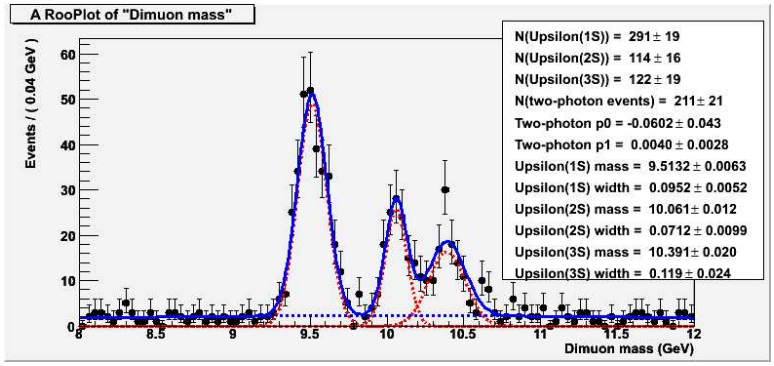

Figure 6: Dimuon invariant mass in the Υ resonances (1S, 2S, 3S) region.

4 Summary

CMS is ready to study hard diffractive processes with the LHC early data, using the large rapidity gap and exclusivity techniques. Monte Carlo studies, assuming low instantaneous luminosities and no pile-up, have shown that with the first $10\,\mathrm{pb}^{-1}$ of data it may be possible to observe $\mathcal{O}(300)$ single diffractively produced di-jets for $\langle|S^2|\rangle = 0.05$. Significant deviations from this expected event yield might allow to put constraints on $\langle|S^2|\rangle$ values. When $100\,\mathrm{pb}^{-1}$ of data becomes available, then it should be possible to observe $\mathcal{O}(100)$ single diffractively produced $W \to \mu\nu$ events, again assuming $\langle|S^2|\rangle = 0.05$. At this point, it may also be possible to observe clear signals of Υ resonances photoproduction and even study some aspects of their production dynamics.

References

[1] The CMS Collaboration, J. Phys. **G34** 995 (2007).

[2] CMS Collaboration, JINST **0803** S08004 (2008).

[3] CMS Collaboration, CMS PAS DIF-07-002 (2007).

[4] CMS Collaboration, CMS PAS FWD-08-002 (2008).

[5] B. E. Cox and J. R. Forshaw, Comput. Phys. Commun. **144** 104 (2002).

[6] H1 Collaboration, A. Aktas et al., Eur. Phys. J. **C48** 715 (2006).

[7] J. Pumplin, D. R. Stump, J. Huston, H. L. Lai, P. Nadolsky and W. K. Tung, JHEP **0207** 012 (2002).

[8] V. A. Khoze, A. D. Martin and M. G. Ryskin, Phys. Lett. **B643** 93 (2006).

[9] T. Sjostrand, S. Mrenna and P. Skands, JHEP **0605** 026 (2006).

[10] J. Alwall et al., JHEP **0709** 028 (2007).

[11] CMS Collaboration, CMS PAS EWK-07-002 (2007).

[12] G. P. Salam and G. Soyez, JHEP **0705** 086 (2007).

[13] J. S. Miller, Eur. Phys. J. **C56** 39 (2008).

[14] CMS Collaboration, CMS PAS DIF-07-001 (2007).

[15] S. R. Klein and J. Nystrand, Phys. Rev. Lett. **92** 142003 (2004);
J. Nystrand, Nucl. Phys. **A752** 470 (2005).

[16] J. A. M. Vermaseren, Nucl. Phys. **B229** 347 (1983).